THESIS FOR THE DEGREE OF LICENTIATE OF ENGINEERING

On Doppler synchronization and localization in single LEO satellite systems for 6G and beyond

André Bezerra de Freitas Diniz

Department of Electrical Engineering
Chalmers University of Technology
Gothenburg, Sweden, 2026

On Doppler synchronization and localization in single LEO satellite systems for 6G and beyond

André Bezerra de Freitas Diniz

Acknowledgments, dedications, and similar personal statements in this thesis reflect the author's own views.

Department of Electrical Engineering
Chalmers University of Technology
SE-412 96 Gothenburg, Sweden
Phone: +46 (0)31 772 1000

Cover:
Concept of a LEO satellite system drawn by a 7 year old.

Printed by Chalmers Digital Printing
Gothenburg, Sweden, April 2026

On Doppler synchronization and localization in single LEO satellite systems for 6G and beyond

André Bezerra de Freitas Diniz
Department of Electrical Engineering
Chalmers University of Technology

Abstract

The evolution of communication systems towards 6G envisions ubiquitous global connectivity, where non-terrestrial networks will be crucial. Low Earth orbit (LEO) satellites are particularly attractive due to favorable propagation characteristics and low latency. However, their high speeds induce severe Doppler shifts, posing synchronization challenges in satellite-to-ground communications. In addition, vulnerabilities in global navigation satellite systems highlight the need for robust localization alternatives, which are fundamental to enable a wide range of use cases. To avoid high complexity and strict synchronization demands of multi-satellite solutions, Doppler-based single-satellite methods offer an attractive, low-requirement alternative. This thesis addresses these challenges by developing novel, standalone methodologies for Doppler shift tracking and Doppler-based user localization in single LEO satellite systems.

We initially address the Doppler shift tracking problem by a multi-step Doppler shift estimation algorithm based on linear estimators. Taking advantage of additional knowledge of Kepler's laws describing satellite motion, a model-based post-processing stage is proposed. Overall, this procedure provides a continuous and smooth curve describing the Doppler shifts over the satellite's pass in degrading channel conditions.

Following, we develop a Doppler-based single-satellite localization algorithm where several impairments are jointly modeled. These are originated due to the receiver's hardware, atmospheric phenomena and imprecise knowledge of the satellite states. Higher accuracy in relation to previously developed methods in the literature, which do not address the combined effect of such perturbations, is shown. As such, our proposed technique may be applied in practical and resource-constrained scenarios.

Keywords: Doppler shift, satellite communications, estimation theory.

Àqueles que acreditaram em mim quando eu não o fiz.

List of Publications

This thesis is based on the following publications:

[A] **André B. de F. Diniz**, Thomas Eriksson, Ulf Gustavsson, "Doppler Shift Estimation for Satellite Communications using Linear Estimators". Published in *25th IEEE Workshop on Signal Processing Advances in Wireless Communications (SPAWC)*, pp. 686-690, 2024.

[B] **André B. de F. Diniz**, Thomas Eriksson, Ulf Gustavsson, "An Algorithm for Harsh Doppler Shift Estimation for Satellite Communications". Published in *58th Asilomar Conference on Signals, Systems & Computers*, pp. 706-710, 2024.

[C] **André B. de F. Diniz**, Thomas Eriksson, Ulf Gustavsson, Sharief Saleh, Henk Wymeersch, Sebastian Euler, "Doppler-based Geolocalization under Hardware, Atmospheric and Orbital Impairments for Single LEO Satellite Systems". Submitted to *IEEE Transactions on Aerospace and Electronic Systems*.

Contents

Acknowledgments

This is actually the first time that I acknowledge (or at least try to) so many people in written form. While this may seem like an easy task, this is probably the most difficult part of this thesis. It's in moments like these that I realize that there are SO many people supporting me over the years and I definitely couldn't be more grateful. I may fail in making justice to everyone, but I promise I'll try my best in doing so.

À minha família, que incondicionalmente me deu todo tipo de suporte e que sempre acreditou em mim quando tudo parecia ter chegado ao seu fim. Não foram poucos os exemplos de paixão, disciplina e, acima de tudo, resiliência. Obrigado imensamente a Eliane, Francisco, Gabriela, Tiago, Juliana, Thaís, Martina e Bella.

Seria injusto não mencionar exemplos que se fizeram presentes desde muito cedo. A Rose, Jorge e Jatobá, que me mostraram o poder de inspirar e dedicar. A Ana Luísa e Isadora, que me deram o privilégio da amizade durante tantos anos. Jamais posso esquecer do meu amigo Yago, com quem sempre poderei compartilhar de tudo (menos o Grammy). Às minhas amigas Bárbara e Carol, por me acompanharem na solitária jornada que é viver longe.

Ao Cilada que primeiro quebrou-me a jarra, dedico com saudosa lembrança esta tese. Aos amigos Theus, Gauss, Marquinho, Silas, Kana, Yan, Baca, Jamaico e Fábio, que navegaram comigo em turbulentas águas.

Muitos também são aqueles que me alçaram a voos mais altos. Especialmente a Danilo e Vicente, deixo meus eternos agradecimentos pelos meus primeiros passos na arte que é pesquisar.

Aos "amigos" brasileiros que tão bem me acolheram desde que cheguei aqui, agradeço pelas constantes risadas, inacreditáveis histórias e incontáveis horas nos karokês da cidade.

Ich könnte auf gar keinen Fall vergessen, etwas über dich zu schreiben, Johanna. Wir haben zusammen so viel durchgemacht und du hast mir in den schlimmsten Zeiten immer einen Weg gezeigt.

Immense kudos to my BOGO friends, MIPA, NEMK and PIPO, for all the joint work and remarkable friendship. I cannot forget being with all of you in such stormy times. You guys made a cozy little place out of a cold and uncertain world. My deepest gratitude to Martin and Pablo, for showing me the light at the end of the tunnel and how to untangle many of the signal processing mysteries.

To my supervisors, Thomas and Ulf, my fullest gratitude. I couldn't have reached this point without your constant support, fierce scientific debates and good laughs in each meeting. It's amazing how much I have grown and I owe a lot of that to you. Sharief, Henk and Sebastian, thank you so much for all the collaboration and patience. I have learned lots from all of you and the lessons I've taken will always be with me. Last but not least, thanks a lot to Henrik for always listening to my needs and guiding me through bumpy roads.

André Diniz
Göteborg, February 2026.

Acronyms

3GPP:	3rd Generation Partnership Project
5G:	Fifth Generation Wireless
6G:	Sixth Generation Wireless
CFO:	carrier frequency offset
CRLB:	Cramér-Rao lower bound
ECEF:	Earth-centered, Earth-fixed
ECI:	Earth-centered inertial
EKF:	extended Kalman filter
GEO:	geostationary Earth orbit
GNSS:	global navigation satellite system
GPS:	global positioning system
HEO:	highly elliptical orbit
LEO:	low Earth orbit
LoS:	line of sight
MEO:	medium Earth orbit
MSE:	mean square error
NTNs:	non-terrestrial networks
OFDM:	orthogonal frequency division multiplexing
PCRB:	posterior Cramér-Rao lower bound
PN:	phase noise
PSS:	primary synchronization signal
RMSE:	root mean square error

RTT:	round trip time
S2G:	satellite-to-ground
SGP4:	Simplified General Perturbations-4
SNR:	signal-to-noise ratio
TNs:	terrestrial networks
UE:	user equipment
WGS84:	World Geodetic System 84
WLS:	weighted least squares

Part I

Overview

CHAPTER 1

Introduction

Though artificial satellites had already been idealized as thought experiments by Sir Isaac Newton in *Philosophiæ Naturalis Principia Mathematica*, it was not until centuries later that the first launch was performed, with the Sputnik 1 in 1957. Ever since, artificial satellites have become a crucial and popular infrastructure component to carry out several tasks, including weather forecasting, navigation, scientific research and communication. The first communication satellite was launched in 1958 within project SCORE, and over the following decades, satellites have shown to be of fundamental importance in providing a commercially viable means to several services within communications, such as telephony, TV broadcasting and rescue systems. As a consequence of their increasing popularity and improved cost effectiveness, it is estimated that 100,000 satellites could be operational by 2030 [1].

Nowadays, satellites have been integrated into Fifth Generation Wireless (5G)-Advanced networks, supporting critical functions such as edge computing, remote monitoring, and vehicle-to-everything communication [2], [3]. As these systems continue to be deployed on a global scale, interest in advancing towards Sixth Generation Wireless (6G) technologies is rapidly growing. One of the main advances of 6G in relation to previous generations is ubiquitous

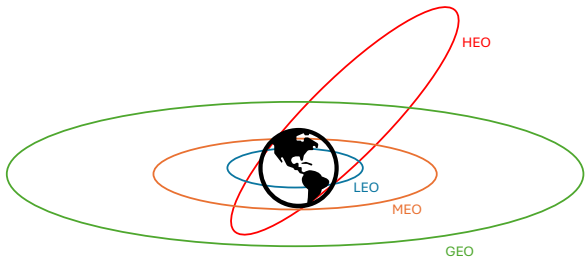

Figure 1.1: Considered orbits for NTNs.

connectivity, serving remote areas either on land or at sea. Another key aspect is that communication, localization and sensing are expected to coexist while simultaneously sharing time, frequency and space resources with improved spectrum efficiency [4]. For these purposes, seamless integration of non-terrestrial networks (NTNs) will be of vital importance [5], [6], [7].

In general, NTNs may contain satellites orbiting at different altitudes, serving either as relays or base stations. According to the 3rd Generation Partnership Project (3GPP), these satellites are divided in low Earth orbit (LEO), medium Earth orbit (MEO), geostationary Earth orbit (GEO) or highly elliptical orbit (HEO), as in Fig. 1.1. These categories embrace orbit altitudes of, respectively, 500-2,000 km, 8,000-20,000 km, 35,786 km and 1,000-35,786 km. In recent years, LEO satellites have surged as an attractive building block for future communication networks due to a variety of factors. In comparison to orbits of higher altitudes, LEO satellites offer better cost effectiveness, more favorable propagation characteristics and shorter delays [8], [9], [10].

Signal propagation with LEO satellites, however, has some significant drawbacks. Due to their high speeds (4-8 km/s), pronounced Doppler shifts during satellite-to-ground (S2G) transmissions arise [11]. In S-band, for instance, they may be in the order of tens of kHz. In multi-carrier systems, these Doppler shifts may cause inter-carrier interference, apart from frequency and time synchronization errors [12], [13]. Consequently, Doppler synchronization becomes crucial for proper operation of upcoming NTNs. Despite constituting a relevant system impairment, Doppler shifts can be measured with low-cost hardware and processed for other applications. As such, one of the main topics addressed by this thesis is synchronization under harsh Doppler.

With the focus on NTNs for 6G and beyond, LEO satellites are expected to play a major role in sensing and localization tasks, further enabling a broad range of use cases, including environmental monitoring and automated transportation [5], [14]. It is anticipated that these satellites will be of great relevance in verification, guaranteeing user privacy, preventing unauthorized access and assuring efficient resource allocation, particularly in remote areas not easily covered by terrestrial networks. For such goals, the global navigation satellite system (GNSS) is a consolidated alternative. This system, however, is subject to significant vulnerabilities, namely jamming, spoofing and interference [15], [16], [17]. Therefore, it becomes important to develop verification solutions that are independent from the traditional GNSS. Doppler shifts can be easily measured and explored for this task, providing the motivation for the second main research work in this thesis [18].

This thesis is structured as follows. In Chapter 2, we discuss the Doppler shift tracking task and develop a system model based on Kepler's laws. Moreover, we examine state-of-the-art methods and their limitations. To circumvent such shortcomings, we develop a model-based Doppler shift tracking technique. In Chapter 3, we address Doppler-based geolocalization in single LEO satellite systems, where we extend the previously developed system model to model the combined effect of a variety of impairments. While state-of-the-art methods model some of these impairments, they are limited in practical applicability since the joint effect of such disturbances is not extensively addressed. To overcome such challenges, we develop a localization algorithm based on the extended system model and improved accuracy is demonstrated. In Chapter 4, the included papers in this thesis are presented and summarized. Finally, conclusions and future research directions are given in Chapter 5.

CHAPTER 2

Doppler shift tracking for LEO satellite-to-ground transmissions

As previously discussed, Doppler shifts are an undesired phenomenon that originate from the relative motion between a satellite and a ground user. To compensate for this effect, Doppler synchronization is a necessary step in the communication system, and so we dedicate the first part of this thesis to this area. In order to comprehend how this can be performed, we start this chapter by describing a basic satellite motion model based on six orbital parameters. Further, we derive an expression for the Doppler shift that involves the user's position and the satellite's orbital parameters. Based on these derivations, we define the Doppler shift tracking problem in the context of satellite-to-ground transmissions. We then summarize state-of-the-art techniques that have been developed for the considered S2G transmission scenario. Finally, we discuss our proposed solution for the Doppler shift tracking task, which overcomes limitations in previously developed methods.

2.1 System model

In this thesis, we focus on a scenario where a single LEO satellite transmits a pilot signal to a ground user equipment (UE) in line of sight (LoS) conditions. As such, in this section we develop a system model to represent the received signals, which are affected by Doppler shifts. This phenomenon originates from the relative motion between the satellite and the UE and is described by a time-varying function $f_d^{(\boldsymbol{\theta}_u, \boldsymbol{\theta}_s)}(t)$, which depends on two parameter sets. The first of them is the UE's position $\boldsymbol{\theta}_u = [\lambda, \phi]^T$, where λ represents the longitude and ϕ the latitude. The second set contains the satellite's orbital parameters $\boldsymbol{\theta}_s$, which governs its motion and is detailed in the following.

2.1.1 Orbital parameters

Satellites travel around the Earth following an ellipsoidal orbit. Their states (position, velocity and so on), at any point in time, are fully described by 6 parameters:

- **eccentricity** (e_c): shape of the ellipse, describing its elongation in relation to a circle;
- **semi-major axis** (a): half of the major axis of the ellipse;
- **inclination** (i): angle between the orbital and equatorial planes;
- **longitude of the ascending node** (Ω): angle from the reference direction to the ascending node (point where the orbit crosses the equatorial plane);
- **argument of periapsis** (ω): angle between the ascending node and the periapsis (where the satellite is the closest to the Earth);
- **true anomaly** (ν): angle between the direction of periapsis and the satellite's position, centered on the ellipsoidal focus.

A basic model of the satellite's states at any time is derived using Kepler's equations [19], [20]. To enable a representation in Earth-centered, Earth-fixed (ECEF) coordinates, which rotates with the Earth and is widely used for orbit tracking, we start with some basic definitions and initially formulate the satellite's motion in the Earth-centered inertial (ECI) coordinate system,

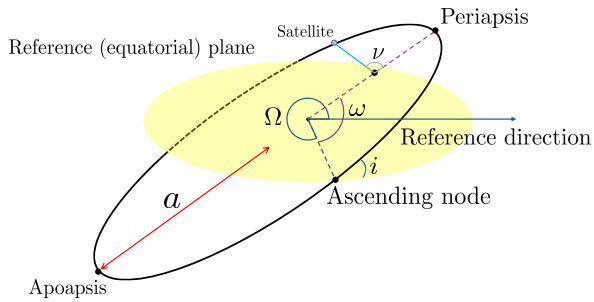

Figure 2.1: Graphical overview of orbital parameters (taken from [22]).

followed by a description of orbital perturbations. The UE's position in the ECEF framework $\mathbf{p}_u^{\boldsymbol{\theta}_u}$ is taken by applying the World Geodetic System 84 (WGS84) Earth model [21].

2.1.2 Keplerian motion

The mass of the Earth M_e is several orders of magnitude larger than that of the satellite. As such, the satellite's mean angular velocity can be reasonably approximated by $n_s = \sqrt{GM_e/a^3}$, where G corresponds to the gravitational constant. For a time instant t, the mean anomaly (fraction of the orbit that has been passed after the satellite reached the periapsis) is calculated by $M = M_0 + n_s(t - t_0)$, where M_0 corresponds to the mean anomaly value at $t = t_0$ [23]. We consider $t_0 = 0$ without loss of generality.

Following, we introduce the eccentric anomaly E (angle between the periapsis and the satellite's position, measured at the ellipsoidal center), which is related to the mean anomaly by $M = E - e_c \sin E$. The solution for E is not found in closed form, but it can be approximated by $E = M + e_c \sin M + \frac{1}{2}e_c^2 \sin(2M) + \frac{1}{8}e_c^3 (3\sin(3M) - \sin M)$ [19]. From this solution, the true anomaly is calculated with $\nu = 2\arctan\left(\tan(E/2)\sqrt{(1+e_c)/(1-e_c)}\right)$. Based on the given expressions, the distance between the satellite and the center of the Earth is calculated by

$$r_s = \frac{a(1-e_c^2)}{1 + e_c \cos\nu}, \tag{2.1}$$

where the time argument is omitted for simplicity of notation.

All the described variables allow the calculation of the position of the satellite in ECI coordinates. Respectively, the (x, y, z) components are

$$\mathbf{p}_{s,\mathrm{ECI}}^{\boldsymbol{\theta}_s}(t) = r_s \begin{bmatrix} \cos(\omega+\nu)\cos\Omega - \sin(\omega+\nu)\sin\Omega\cos i \\ \cos(\omega+\nu)\sin\Omega + \sin(\omega+\nu)\cos\Omega\cos i \\ \sin(\omega+\nu)\sin i \end{bmatrix}. \tag{2.2}$$

The velocity is taken by deriving (2.2) with relation to time, giving

$$\mathbf{v}_{s,\mathrm{ECI}}^{\boldsymbol{\theta}_s}(t) = \frac{n_s a}{r_s} \begin{bmatrix} bl_2\cos E - al_1\sin E \\ bm_2\cos E - am_1\sin E \\ bn_2\cos E - an_1\sin E \end{bmatrix}, \tag{2.3}$$

with

$$\begin{aligned} b &= a\sqrt{1-e_c^2}, \\ l_1 &= \cos\Omega\cos\omega - \sin\Omega\sin\omega\cos i, \\ m_1 &= \sin\Omega\cos\omega + \cos\Omega\sin\omega\cos i, \\ n_1 &= \sin\omega\sin i, \\ l_2 &= -\cos\Omega\sin\omega - \sin\Omega\cos\omega\cos i, \\ m_2 &= -\sin\Omega\sin\omega + \cos\Omega\cos\omega\cos i, \\ n_2 &= \cos\omega\sin i. \end{aligned}$$

The satellite's position in ECEF coordinates $\mathbf{p}_s^{\boldsymbol{\theta}_s}(t)$ is calculated by $\mathbf{p}_s^{\boldsymbol{\theta}_s}(t) = \mathbf{T}\mathbf{p}_{s,\mathrm{ECI}}^{\boldsymbol{\theta}_s}(t)$, where

$$\mathbf{T} = \begin{bmatrix} \cos\theta & \sin\theta & 0 \\ -\sin\theta & \cos\theta & 0 \\ 0 & 0 & 1 \end{bmatrix}, \tag{2.4}$$

where $\theta = \theta_0 + \omega_e t$. Further, θ_0 denotes the Greenwich sidereal time at 0h UT and ω_e the Earth's angular speed. Applying the chain rule, the satellite's velocity in ECEF coordinates is $\mathbf{v}_s^{\boldsymbol{\theta}_s}(t) = \mathbf{T}\mathbf{v}_{s,\mathrm{ECI}}^{\boldsymbol{\theta}_s}(t) + \dot{\mathbf{T}}\mathbf{p}_{s,\mathrm{ECI}}^{\boldsymbol{\theta}_s}(t)$, with

$$\dot{\mathbf{T}} = \begin{bmatrix} -\omega_e\sin\theta & \omega_e\cos\theta & 0 \\ -\omega_e\cos\theta & -\omega_e\sin\theta & 0 \\ 0 & 0 & 0 \end{bmatrix}. \tag{2.5}$$

States of higher order, e.g., acceleration, may be calculated numerically.

Orbital perturbations

In practice, the Simplified General Perturbations-4 (SGP4) model is broadly used to propagate satellite orbits. Due to many factors acting over the satellite, including atmospheric drag and solar radiation pressure, this model may not be entirely accurate in describing the satellite's position and velocity [24], [25]. Orbital perturbations generate errors in the satellite's argument of latitude $\beta = \omega + \nu$, defined as the angle between the ascending node and the satellite. As LEO satellites follow a nearly circular orbit, for an along-track error of magnitude ε, we approximate the perturbed argument of latitude by $\tilde{\beta} = \omega + \nu + \arcsin(\varepsilon/a)$ [26], [27].

Several studies have shown that, despite daily updates of the orbital parameters, orbital perturbations may yield position prediction errors of up to 3 km, concentrated along the track of the satellite's orbit. Also, velocity prediction errors are concentrated in the radial direction, usually between 4-10 m/s [27], [28].

2.1.3 Doppler shift formulation

From the described satellite motion model, we derive an expression relating Doppler shifts to the satellite's states to later define a representation for the received signals in the analyzed S2G transmissions. We start with a continuous-time passband signal transmitted by the satellite to the UE [29]

$$s_{\mathrm{RF}}(t) = 2\mathrm{Re}\{s(t)e^{j2\pi f_c t}\}, \tag{2.6}$$

with $s(t)$ denoting the complex baseband signal, f_c the carrier frequency and $\mathrm{Re}\{\cdot\}$ the real part of a complex number. Assuming a single path and noiseless channel, the received passband signal is given by

$$r_{\mathrm{RF}}(t) = 2\mathrm{Re}\{D(t)s(t - \tau^{(\boldsymbol{\theta}_u,\boldsymbol{\theta}_s)}(t))e^{j2\pi f_c(t-\tau^{(\boldsymbol{\theta}_u,\boldsymbol{\theta}_s)}(t))}\}, \tag{2.7}$$

where we introduce the amplitude $D(t)$ due to free space loss and the time-varying delay $\tau^{(\boldsymbol{\theta}_u,\boldsymbol{\theta}_s)}(t)$. The latter is a function of the UE's and the satellite's

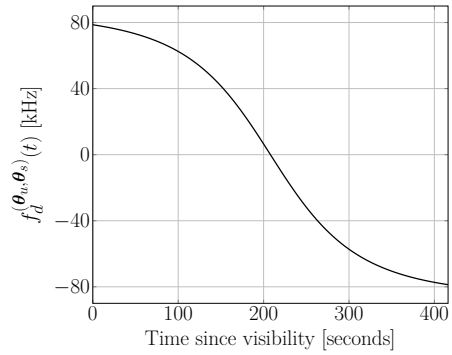

Figure 2.2: Example of Doppler shifts over a satellite pass representing a S-curve.

position, and is given by

$$\tau^{(\boldsymbol{\theta}_u,\boldsymbol{\theta}_s)}(t) = \frac{||\mathbf{p}_u^{\boldsymbol{\theta}_u} - \mathbf{p}_s^{\boldsymbol{\theta}_s}(t)||}{c} = \frac{\sqrt{\left[\mathbf{p}_u^{\boldsymbol{\theta}_u} - \mathbf{p}_s^{\boldsymbol{\theta}_s}(t)\right]^T \left[\mathbf{p}_u^{\boldsymbol{\theta}_u} - \mathbf{p}_s^{\boldsymbol{\theta}_s}(t)\right]}}{c}$$
$$= \frac{\sqrt{||\mathbf{p}_u^{\boldsymbol{\theta}_u}||^2 - 2\mathbf{p}_s^{\boldsymbol{\theta}_s T}(t)\mathbf{p}_u^{\boldsymbol{\theta}_u} + ||\mathbf{p}_s^{\boldsymbol{\theta}_s}(t)||^2}}{c}, \tag{2.8}$$

where c represents the speed of light.

It can be seen in (2.7) that the time variations of the delay induce phase rotations at the receiver of $-f_c\tau^{(\boldsymbol{\theta}_u,\boldsymbol{\theta}_s)}(t)$. The Doppler shift is defined as their first-order time variation, giving

$$f_d^{(\boldsymbol{\theta}_u,\boldsymbol{\theta}_s)}(t) = -f_c\frac{\partial\tau^{(\boldsymbol{\theta}_u,\boldsymbol{\theta}_s)}(t)}{\partial t} = \frac{f_c}{c}\frac{\mathbf{v}_s^{\boldsymbol{\theta}_s T}(t)\left[\mathbf{p}_u^{\boldsymbol{\theta}_u} - \mathbf{p}_s^{\boldsymbol{\theta}_s}(t)\right]}{||\mathbf{p}_u^{\boldsymbol{\theta}_u} - \mathbf{p}_s^{\boldsymbol{\theta}_s}(t)||}. \tag{2.9}$$

Due to the shape of $f_d^{(\boldsymbol{\theta}_u,\boldsymbol{\theta}_s)}(t)$ during a satellite pass, this function is usually referred to as "S-curve". An example is given in Fig. 2.2.

2.1.4 Received signal model

In our study, we consider the transmission of signals from a LEO satellite to a static UE in continuous strong LoS conditions such that the Doppler shift description from (2.9) is valid over the satellite's pass. The transmitted signals consist of packets containing pilot and data symbols. The packets

have a duration T_r and are transmitted at slow-time epochs $m = 0, \ldots, M$, with $M = \lceil T_p/T_r \rceil - 1$ and $T_p = MT_r$ denoting the duration of the satellite pass. For a sampling period T_s, the pilot blocks have a duration LT_s, with L representing the amount of pilot symbols. The transmission-reception scheme is illustrated in Fig. 2.3.

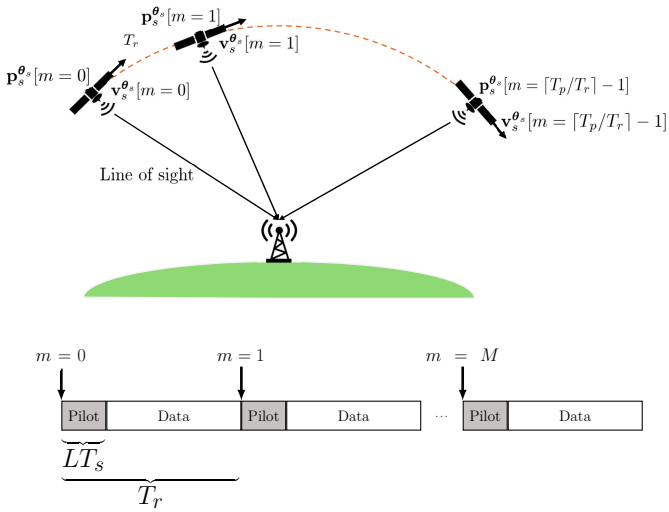

Figure 2.3: Transmission-reception scheme and structure of the transmitted packets. Each pilot block is transmitted every T_r seconds during the satellite pass. Respectively, $\mathbf{p}_s^{\boldsymbol{\theta}_s}[m]$ and $\mathbf{v}_s^{\boldsymbol{\theta}_s}[m]$ denote the satellite's position and velocity at the transmission of the m^{th} pilot block (adapted from [30]).

The pilot blocks, which in this case are all-ones vectors, are short enough so that the Doppler shift $f_d = f_d^{(\boldsymbol{\theta}_u, \boldsymbol{\theta}_s)}(t)$ is approximately constant over their entire duration. A constant uniformly random phase shift $\varepsilon_m \sim \mathcal{U}[0, 2\pi]$ is also present. Based on [31], [32] and the system illustrated in Fig. 2.3, we write the m^{th} received pilot block as

$$y_{m,n} = D_m e^{j(\varepsilon_m + \Omega_d n)} x_n + w_n, \; n = 0, \ldots, L-1. \tag{2.10}$$

For a sampling frequency f_s, we represent $\Omega_d = 2\pi f_d / f_s$, $w_n \sim \mathcal{CN}(0, \sigma_w^2)$ and the signal amplitude as D_m.

2.2 Doppler shift tracking for LEO satellite systems

From the described system model, we define the Doppler shift tracking problem as estimating $f_d^{(\boldsymbol{\theta}_u,\boldsymbol{\theta}_s)}(t)$ for the entire satellite pass with knowledge of the UE parameters $\boldsymbol{\theta}_u$. The precise estimation of $\boldsymbol{\theta}_s$ is not of particular interest in the tracking task, as we are not concerned about determining the satellite's motion.

As a crucial step in S2G transmissions [33], 3GPP has defined accuracy requirements for the Doppler shift tracking. To comply with them, several techniques have been developed for the considered transmission-reception scenario. The study in [32] explores, in addition to pilot blocks (termed explicit pilots), data from signals publicly broadcasted by the satellite. The signals from public broadcasts usually contain interleaved or consecutive zeros and ones, are affected by the same Doppler shifts of the explicit pilots and are termed implicit pilots. After proper identification, the additional data gathered from the implicit pilots is used to estimate Doppler shifts with higher accuracy than using only explicit pilots. This method, however, heavily relies on phase unwrapping, consequently deviating from the Cramér-Rao lower bound (CRLB) at relatively high signal-to-noise ratio (SNR) levels [34].

The technique in [31] applies turbo codes and Gaussian process models to estimate Doppler shifts. First, the soft outputs of the turbo decoder for a few number of Doppler shifts are evaluated and modeled by a Gaussian process, reducing the complexity of exhaustive evaluation for many candidate Doppler shifts. Then, the Newton-Raphson method is applied to give an initial coarse estimate. A refinement is performed through maximum likelihood estimation.

In general, in the literature, Doppler shifts at a certain time are estimated by applying an estimation algorithm over a received pilot block. However, even with estimators that approach the CRLB, such procedure may still yield a noisy S-curve, as shown in Fig. 2.4. This is due to the fact that such reconstruction is based *only* on Doppler shift estimates. Especially in very noisy environments, this may represent a significant loss in service quality. To address this challenge, we propose a model-based solution in the following.

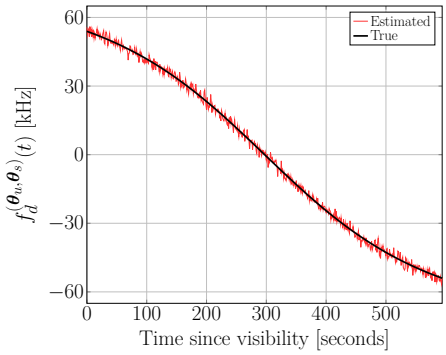

Figure 2.4: Example of true and estimated Doppler shifts over a satellite pass without post-processing ($L = 500$, $f_c = 4$ GHz, SNR $= -5$ dB).

2.2.1 Model-based post-processing

In order to yield a smooth S-curve in degrading noise conditions and further reduce the error between estimated and true Doppler shifts, our proposed solution comprises two main stages:

- estimation of Doppler shifts using a sequence of linear estimators;
- estimation of the satellite's parameters and application to the model defined in (2.9).

Based on classical estimation theory, the first stage is performed using a sequence of linear estimators, which are shown to approach the CRLB for a broad range of SNR levels. Details about this step and performance are given in [35]. Our contribution lies in the second stage, comprising a *post-processing* procedure based on the Keplerian motion model discussed in Section 2.1.2.

We consider the system illustrated in Fig. 2.3, where each received pilot block is used to yield a Doppler shift estimate. As such, $M + 1$ Doppler shift estimates are available, stored in the vector $\hat{\mathbf{f}}_d$. This vector is used to estimate the satellite's orbital parameters $\boldsymbol{\theta}_s$ through the least squares solution

$$\hat{\boldsymbol{\theta}}_s = \arg\min_{\boldsymbol{\theta}_s} \left\| \hat{\mathbf{f}}_d - \mathbf{f}_d(\boldsymbol{\theta}_u, \boldsymbol{\theta}_s) \right\|^2. \tag{2.11}$$

In this problem, the vector $\mathbf{f}_d(\boldsymbol{\theta}_u, \boldsymbol{\theta}_s)$ denotes the Doppler shifts generated by the models described in Sections 2.1.2 and 2.1.3 for the time of the pilot

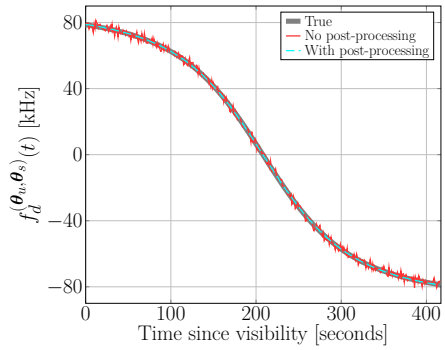

Figure 2.5: Example of true and estimated Doppler shifts, with and without post-processing, over a satellite pass ($L = 500$, $f_c = 4$ GHz, SNR $= -5$ dB).

block receptions. Since the UE's position (contained in $\boldsymbol{\theta}_u$) is known, the only unknown parameter set is $\boldsymbol{\theta}_s$. The respective solution is used to generate a smooth S-curve $f_d^{(\boldsymbol{\theta}_u,\hat{\boldsymbol{\theta}}_s)}(t)$ as in Fig. 2.5.

The performance improvement comes from the additional knowledge of the satellite motion model. Such approach may be used in conjunction with the exploitation of signal structures, such as those of orthogonal frequency division multiplexing (OFDM) signals, leading to further improvements.

We note that the estimate $\hat{\boldsymbol{\theta}}_s$ may be far from the true one. This is due to the satellite motion model itself, which is not particularly sensitive to the parameters defining $\boldsymbol{\theta}_s$. Physically, this means that several orbits generate similar Doppler shifts over the same satellite pass time. Nevertheless, we accept those solutions as we are concerned only with tracking the respective Doppler shifts. An example is given in Fig. 2.6.

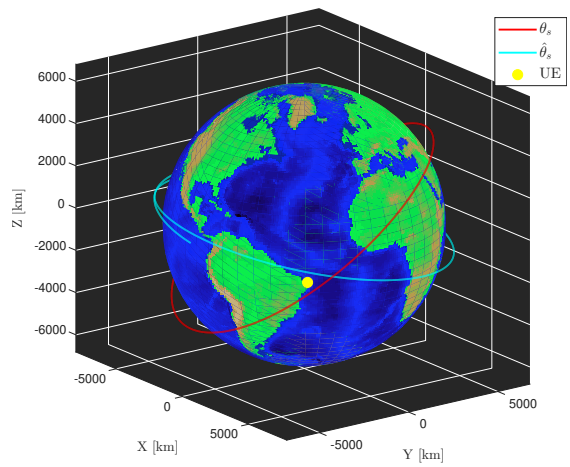

Figure 2.6: Example of true and estimated satellite paths yielding similar Doppler shifts.

CHAPTER 3

Doppler-based user localization for single LEO satellite systems

In order to ensure continuous service anytime and anywhere in 6G networks, NTNs will serve as a complement to terrestrial ones. Due to favorable channel conditions in relation to satellites in higher orbits and lower mission costs, LEO satellites have gained popularity over the years for the implementation of several services. One such service is user verification, defined as asserting the consistency of a certain UE position with physical layer observations and system constraints, without necessarily determining the user's exact location. Over the years, verification has been extensively performed by GNSS, which operates at medium Earth orbit and is susceptible to jamming, spoofing and other vulnerabilities. Verification can also be performed with LEO satellite constellations, however at the cost of high computational complexity and strict inter-satellite synchronization. In contrast, the same task can be performed with only one satellite, relaxing such requirements. In this context, Doppler shifts may be utilized, given the involved geometrical dependencies and ease of measurements. Motivated by these practicalities, we discuss how Doppler shifts in single LEO satellite systems can be used for user verification, independent from GNSS. Following, we extend the system model developed in

Sections 2.1.2-2.1.4 to address realistic impairments that arise at the receiver hardware and the channel. Finally, we give an overview of our algorithm for user verification that accounts for such effects.

3.1 Localization beyond GNSS

Over the years, UE localization in satellite systems has been carried out using a wide variety of measurement types, such as round trip time (RTT), delay and range-difference [36], [37]. Doppler shifts may also be used for the same purpose: from known satellite parameters $\boldsymbol{\theta}_s$, Doppler shifts can be directly related to the UE's position $\boldsymbol{\theta}_u$ as seen in (2.9). One benefit of using this type of data lies on the possibility of measurement with simple hardware, therefore being attractive to applications with limited resources [18].

Research on Doppler-based UE localization can be traced back to at least the 1960's, which subsequently led to the development of the TRANSIT and global positioning systems (GPS) [38], [39]. Other constellations have been later deployed that take advantage of Doppler shift measurements for localization purposes, including Globalstar and Iridium [15], [37], [40]. Nevertheless, GNSS has become the most widespread system for localization and is integrated into 3GPP specifications [41]. However, such system has demonstrated vulnerability to jamming, interference and spoofing [15], [16], [17]. Consequently, user verification may be significantly threatened, possibly leading to data breaches and unauthorized accesses. As such, interest towards standalone localization solutions has increased, with the increasingly popular LEO satellites emerging as an attractive alternative to reduce GNSS dependence.

3.2 Single LEO- and Doppler-based localization

Similar to the problem addressed in Section 2.2, we also aim at extracting information from Doppler shifts. For the localization task, estimated Doppler shifts are used as a means to estimate the UE parameters $\boldsymbol{\theta}_u$. In this context, verification solutions have been developed that apply LEO satellite constellations. These techniques, however, have high computational complexity and demand precise inter-satellite synchronization. In contrast, the same task can be performed in single satellite systems, which simplify or even eliminate such requirements. For this purpose, approximate knowledge of the satellite states

(due to orbital perturbations) is available [32], [42].

In [2], [43], 3GPP has defined a 10 km user verification accuracy requirement for single LEO satellite systems. To comply with this benchmark, several techniques have been developed to perform Doppler-based user verification in the same transmission-reception scenario considered in this thesis, illustrated in Fig. 2.3. Despite the development of localization methods that address different hardware impairments, studies that consider the *joint* effect of more realistic perturbations have not been extensively conducted. For example, the method in [44] does not model carrier frequency offset (CFO) and the satellite position errors are in the scale of meters, when these in GNSS-free scenarios may be in the order of kilometers, as discussed in Section 2.1.2. In [45] no Doppler tracking technique is developed, which may turn the method limited in terms of applicability since the phase may be strongly affected by phase noise (PN). Also, a spherical model of the Earth is assumed, which may yield relevant positioning errors. Based on such limitations, in the following we develop a localization technique addressing the combined effect of realistic impairments in practical communication systems.

3.2.1 Localization under hardware, atmospheric and orbital impairments

To overcome the limitations from previous studies, in [30] we develop a standalone user verification technique for realistic single LEO satellite environments. By jointly modeling a variety of orbital, atmospheric and hardware impairments, we extend the system model discussed in Sections 2.1.2-2.1.4. Moreover, we define a tracking parameter originating from Doppler shifts that can be used to estimate the UE's position. Finally, accuracy improvements with respect to state-of-the-art methods for Doppler shift tracking and localization are achieved.

Continuous-time system model

The transmission-reception scheme is the same as that described in Section 2.1.4, with the satellite broadcasting its orbital parameters $\boldsymbol{\theta}_s$. We model the

continuous-time complex baseband pilot block as [29]

$$s(t) = \sum_{n=0}^{L-1} z_n h(t - nT_s), \tag{3.1}$$

where z_n represents a pilot symbol with $|z_n| = 1$ and $h(t)$ a Nyquist pulse. Following, the m^{th} real-valued passband pilot block is given by

$$s_{m,\text{RF}}(t) = 2\text{Re}\{s(t - mT_r)e^{j2\pi f_c(t-mT_r)}\}. \tag{3.2}$$

The signal $s_{m,\text{RF}}(t)$ propagates through a LoS channel and suffers free space path loss. Moreover, the signal suffers a propagation delay $\Delta(t)$ with a geometric contribution $\tau^{(\boldsymbol{\theta}_u,\tilde{\boldsymbol{\theta}}_s)}(t)$ as defined in (2.8) and an atmospheric one $\xi_{\text{at}}(t)$ due to ionospheric and tropospheric effects, such that

$$\Delta(t) = \tau^{(\boldsymbol{\theta}_u,\tilde{\boldsymbol{\theta}}_s)}(t) + \xi_{\text{at}}(t), \tag{3.3}$$

where $\tilde{\boldsymbol{\theta}}_s$ denotes the satellite parameters with a perturbed argument of latitude $\tilde{\beta}$ (see Section 2.1.2). Accounting for attenuation and propagation delays, the m^{th} received passband signal is written as

$$r_{m,\text{RF}}(t) = 2D_m\text{Re}\Big\{s(t - mT_r - \Delta(t))e^{j2\pi f_c(t-mT_r-\Delta(t))}\Big\}, \tag{3.4}$$

with D_m denoting its amplitude.

The signal $r_{m,\text{RF}}(t)$ is downconverted by a receiver whose local oscillator adds a CFO η and PN $\gamma(t)$. The CFO is modeled as a constant phase rotation per time unit and PN as a Wiener process, where $\gamma(0) \sim \mathcal{U}[0, 2\pi]$ [46], [47], [48]. In practice, the hardware may add other distortions over the received signals, such as IQ imbalance or nonlinearities. However, many of these additional impairments may be generally modeled as constant phase shifts, which do not affect the results in our development. As such, the received passband signal is downconverted by $e^{-j2\pi(f_c+\eta)t}e^{j\gamma(t)}$, which after lowpass filtering gives the m^{th} received complex baseband signal

$$r_m(t) = D_m s(t - mT_r - \Delta(t))e^{j\alpha_m(t)} + n(t), \tag{3.5}$$

with $n(t)$ as additive thermal noise and the phase

$$\alpha_m(t) = -2\pi\left[f_c(mT_r + \Delta(t)) + t\eta\right] + \gamma(t). \tag{3.6}$$

In the following derivations, we denote $\Delta[\cdot]$, $\tau^{(\boldsymbol{\theta}_u,\boldsymbol{\theta}_s)}[\cdot]$ and $\xi_{\text{at}}[\cdot]$, respectively as propagation, geometric and atmospheric delays evaluated at the time inside the square brackets.

Discrete-time system model

We assume that the receiver tracks the block's time of arrival, which is match-filtered and sampled at $t = mT_r + nT_s + \Delta[mT_r]$. This sampling of $r_m(t)$, defined in (3.5), yields

$$r_{m,n} = D_m z_n e^{j\alpha_{m,n}} + w_{m,n}, \tag{3.7}$$

with $w_{m,n}$ denoting additive white Gaussian noise with variance σ_w^2. Since the carrier frequency is usually much larger than the sampling frequency, propagation delay variations within one block do not cause relevant changes in the signal envelope. Instead, with the additional CFO, the propagation delay variations cause relevant phase rotations (as a consequence of Doppler shifts). Evaluating the propagation delays at $mT_r + nT_s$, the additional phase components of $r_{m,n}$ are given by

$$\begin{aligned}\alpha_{m,n} = -2\pi\Big[&f_c(mT_r + \Delta[mT_r + nT_s]) \\ &+ (mT_r + nT_s + \Delta[mT_r + nT_s])\eta\Big] + \gamma_{m,n},\end{aligned} \tag{3.8}$$

where the discrete-time PN $\gamma_{m,n}$ is now included.

It can be seen in the representation in (3.8) that the phase of the received signals contains information regarding the UE's position. This is due to the presence of the propagation delays, which in turn depend on the UE's parameters $\boldsymbol{\theta}_u$, as seen in (3.3). To allow a proper phase analysis, we eliminate the phase contribution from the pilot symbols z_n by

$$y_{m,n} = r_{m,n} z_n^* = D_m e^{j\alpha_{m,n}} + w'_{m,n}, \tag{3.9}$$

redefining the model for the discrete-time received signals in (2.10). The statistical properties of the additive noise are preserved since $|z_n| = 1$.

The derived phase terms in (3.8) may be expressed as a polynomial in n, enabling a simplified analysis and the definition of parameters related to the UE's position. With a Taylor series expansion, we rewrite $\alpha_{m,n}$ as

$$\alpha_{m,n} = A_m + B_m n + O(n^2) + \gamma_{m,n}. \tag{3.10}$$

Terms with order higher than 1 are numerically insignificant, which may only be tracked in very low noise conditions, and so are neglected. Nevertheless, a first-order representation provides a good approximation of $\alpha_{m,n}$ [30].

Based on this reformulated representation, A_m is easily calculated by applying $n = 0$ to (3.8), resulting

$$A_m = -2\pi(f_c + \eta)(mT_r + \Delta[mT_r]). \tag{3.11}$$

This coefficient, however, is corrupted by PN since $\gamma_{m,0} \sim \mathcal{U}[0, 2\pi]$. Therefore, relevant information in estimated values of A_m is lost. However, B_m is not corrupted and can be formulated from $\alpha_{m,n} - \alpha_{m,n-1}$ for any n. Taking this difference for $n = 1$ and $n = 0$, it follows that

$$B_m = -2\pi \left[(f_c + \eta)(\Delta[mT_r + T_s] - \Delta[mT_r]) + T_s\eta\right]. \tag{3.12}$$

Thus, B_m is shown to be the parameter of interest given its dependence on propagation delays. By collecting estimates of B_m over the satellite's pass, it is therefore possible to estimate the UE's position.

UE localization estimation

In [30], we develop an extended Kalman filter (EKF) to track $\alpha_{m,n}$ and B_m. The EKF approaches the posterior Cramér-Rao lower bound (PCRB) for a large range of SNR levels and PN innovation variances.

We start the description of the proposed algorithm by introducing the vector $\mathbf{b}_c^{(\eta,\lambda,\phi)}$, which, based on (3.12), formulates the B_m coefficients as a function of η, λ and ϕ for $m = 0$ up to the current epoch m_c. Each element of this vector is given by

$$b_m^{(\eta,\lambda,\phi)} = -2\pi \left[(f_c + \eta)(\tau^{(\boldsymbol{\theta}_u,\boldsymbol{\theta}_s)}[mT_r + T_s] - \tau^{(\boldsymbol{\theta}_u,\boldsymbol{\theta}_s)}[mT_r]) + T_s\eta\right]. \tag{3.13}$$

This proposition differs from that in (3.12) in two ways. First, only the geometric delays accounted for in (3.13), due to lack of knowledge regarding the atmospheric delays, which may be compensated with specific hardware or with additional information from GNSS [49], [50]. Both are assumed to be not available in our study. Second, we assume unperturbed satellite states (hence the notation $\boldsymbol{\theta}_s$). Without additional information, it is shown in [30] that the along-track position shift ε may only be accurately estimated in very low noise conditions. As such, we perform the optimization without correcting the satellite parameters. The performance of the localization algorithm, however, is not significantly affected despite the presence of orbital perturbations.

Storing the estimates of B_m in the vector $\hat{\mathbf{b}}_c$, we propose a weighted least squares (WLS) solution to the latest estimates of η, λ and ϕ as

$$(\hat{\eta}_c, \hat{\lambda}_c, \hat{\phi}_c) = \underset{\eta,\lambda,\phi}{\arg\min} \big(\hat{\mathbf{b}}_c - \mathbf{b}_c^{(\eta,\lambda,\phi)}\big)^T \mathbf{G}_c^{-1} \big(\hat{\mathbf{b}}_c - \mathbf{b}_c^{(\eta,\lambda,\phi)}\big). \tag{3.14}$$

Here, $\mathbf{G}_c$ is a diagonal matrix with the latest predicted state error covariances of $\hat{B}_m$, extracted from the EKF for $m = 0$ up to m_c. Also, the solution in (3.14) may be found using iterative optimization methods, such as the Nelder-Mead algorithm. Overall, the proposed localization method is summarized in Algorithm 1.

Algorithm 1 UE position estimation algorithm

1: Run EKF as in [30]
2: Store estimates $\hat{B}_m$ in $\hat{\mathbf{b}}_c$ (see (3.12))
3: **if** current epoch $m_c < 2$ **then**
4: **exit**
5: **else if** current epoch $m_c = 2$ **then**
6: Solve (3.14) by coarse-to-fine grid search, yield $(\hat{\eta}_c, \hat{\lambda}_c, \hat{\phi}_c)$ [51]
7: **else**
8: Solve (3.14) using the previous solution $(\hat{\eta}_{c-1}, \hat{\lambda}_{c-1}, \hat{\phi}_{c-1})$ as starting point, yield $(\hat{\eta}_c, \hat{\lambda}_c, \hat{\phi}_c)$
9: **end if**

Algorithm performance

We compare the performance of our developed method to techniques for estimation of B_m and Doppler-based localization in Fig. 3.1. This comparison is performed in terms of the mean distance error over time $\overline{d}_e(t)$ between the estimated and the true UE positions for 1000 Monte Carlo simulations. These were conducted for a minimum SNR of 15 dB (when the satellite is the furthest away from the UE) and a strong PN innovation variance of 5×10^{-4}. The verification requirement given in [2], [43] is also shown.

The first comparison we conduct relates to solution of (3.14) with two different methods for estimation of the B_m coefficients, namely the proposed EKF and the sequence of linear estimators developed in [35]. The latter approaches the CRLB for a wide range of SNR regimes. However, PN is not modeled and

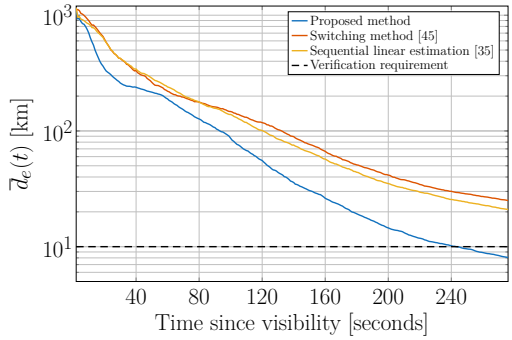

Figure 3.1: Mean distance error over time for different methods ($T_r = 1$ second, $L = 4000$, no orbital perturbations, taken from [30]).

the only impairment is additive noise. As such, PN strongly reduces the accuracy of the UE's position estimates and the verification requirement is not complied with. However, by effectively addressing PN through the EKF, more accurate estimates of B_m are applied to the WLS solution and so the verification requirement is reached.

The performance of the switching method developed in [45] (using the sensitivity parameter $N = 2$), which models CFO, has also demonstrated lower accuracy results. In our simulations, this algorithm is applied with CFO-affected Doppler shift estimates and estimation error variances taken from the technique in [35]. In general, the error from the switching method is higher than that yielded by the solution of (3.14). This is due to the spherical Earth model used to formulate derivatives and error covariance matrices, which when applied to the more accurate WGS84 model (used in our study) gives additional errors.

CHAPTER 4

Summary of included papers

This chapter provides a summary of the included papers.

4.1 Paper A

André B. de F. Diniz, Thomas Eriksson, Ulf Gustavsson
Doppler Shift Estimation for Satellite Communications using Linear Estimators
Published in *25th IEEE Workshop on Signal Processing Advances in Wireless Communications (SPAWC)*, pp. 686-690, 2024.

This conference contribution presents an algorithm for estimation of Doppler shifts in S2G transmissions based on a sequence of linear estimators. These are applied over a linearized version of received pilot signals. Starting with short blocks, the linear estimators are applied and the Doppler shifts are compensated for with the found estimates. After this compensation, the linearization becomes valid for longer blocks and the procedure is repeated, further reducing estimator bias and mean square error. The advantage of such procedure lies

on ease of implementation and predictable behavior. Cramér-Rao bounds are derived and simulations demonstrate that the proposed estimator approaches them for a wide SNR range.

4.2 Paper B

André B. de F. Diniz, Thomas Eriksson, Ulf Gustavsson
An Algorithm for Harsh Doppler Shift Estimation for Satellite Communications
Published in *58th Asilomar Conference on Signals, Systems & Computers*, pp. 706-710, 2024.

This article extends the algorithm in [35] for the case where the normalized Doppler shifts are relatively high, which is the case for low sampling frequencies. This renders the aforementioned linearizations valid only for very short blocks and so the previously developed method is not applicable. To overcome this problem, a model-based estimation of the satellite's orbital parameters is performed to perform Doppler shift pre-compensation. Results show compliance with Cramér-Rao bounds, particularly where the method in [35] fails.

4.3 Paper C

André B. de F. Diniz, Thomas Eriksson, Ulf Gustavsson, Sharief Saleh, Henk Wymeersch, Sebastian Euler
Doppler-based Geolocalization under Hardware, Atmospheric and Orbital Impairments for Single LEO Satellite Systems
Submitted to *IEEE Transactions on Aerospace and Electronic Systems*.

An algorithm for Doppler-based UE localization is presented, jointly modeling several impairments that may affect system performance in practical scenarios. A comprehensive system model is developed, accounting for hardware, atmospheric and orbital perturbations. Simulations show improved accuracy in respect to other state-of-the-art methods for localization and frequency estimation. Moreover, establishing 3GPP verification accuracy requirements as

a benchmark, robustness to degrading channel conditions and imprecise satellite state information is demonstrated.

CHAPTER 5

Concluding Remarks and Future Work

The integration of LEO satellites into NTNs is expected to be crucial in achieving ubiquitous connectivity in future 6G systems. However, the high orbital velocities of LEO satellites introduce severe Doppler shifts, posing significant challenges for S2G communications. Moreover, to enable several applications in future systems, UE localization must be performed in resource-constrained scenarios. In this thesis, we address these challenges by presenting novel methodologies for both Doppler shift tracking and Doppler-based user localization in single LEO satellite systems.

In the context of Doppler synchronization, to overcome the limitations of different methods in the literature, a model-based post-processing solution was proposed. By sequentially applying linear estimators for Doppler shifts followed by satellite orbital parameter estimation (based on the Keplerian motion model), our developed method successfully reconstructs smooth S-curves. This approach significantly reduces the error between estimated and true Doppler shifts, even in strong noise environments.

Furthermore, this thesis explored the application of Doppler shifts for UE localization, offering an alternative to traditional GNSS, which are increasingly vulnerable to jamming and spoofing. While existing studies address isolated

hardware impairments at the receiver side, they often lack comprehensive modeling for combined practical impairments. Consequently, a robust localization algorithm was developed to account for joint hardware, atmospheric, and orbital impairments. This approach utilizes an EKF to track phase parameters from the received signals, followed by a WLS to estimate the UE's position. Simulations of practical scenarios demonstrate that the proposed algorithm successfully meets 3GPP verification accuracy requirements for single LEO satellite systems, whereas other methods fail to do so.

Future research directions in terms of Doppler shift tracking and Doppler-based localization may include the modeling of a moving user, multipath channels and non-LoS propagation conditions. For such purpose, the development of array-based algorithms which address additional impairments (such as self-interference) may be proposed for implementation in practical scenarios.

References

[1] U. S. Agency. "Executive summary: Expanding frontiers." Accessed: October 23, 2025. [Online]. Available: https://www.gov.uk/government/publications/expanding-frontiers-the-down-to-earth-guide-to-investing-in-space/executive-summary-expanding-frontiers.

[2] 3GPP, "Release 18 Description; summary of Rel-18 work items," 3rd Generation Partnership Project (3GPP), Technical Specification (TS) 21.918, Mar. 2025, Version 18.0.0.

[3] K. Ntontin et al., "A vision, survey, and roadmap toward space communications in the 6G and beyond era," *Proceedings of the IEEE*, pp. 1–37, 2025.

[4] M. M. Azari et al., "Evolution of non-terrestrial networks from 5G to 6G: A survey," *IEEE Communications Surveys & Tutorials*, vol. 24, no. 4, pp. 2633–2672, 2022.

[5] H. Pennanen, T. Hänninen, O. Tervo, A. Tölli, and M. Latva-Aho, "6G: the intelligent network of everything," *IEEE Access*, vol. 13, pp. 1319–1421, 2025.

[6] S. Prasad Tera, R. Chinthaginjala, G. Pau, and T. Hoon Kim, "Toward 6G: an overview of the next generation of intelligent network connectivity," *IEEE Access*, vol. 13, pp. 925–961, 2025.

[7] C. T. Nguyen et al., "Emerging technologies for 6G non-terrestrial-networks: from academia to industrial applications," *IEEE Open Journal of the Communications Society*, vol. 5, pp. 3852–3885, 2024.

[8] G. Araniti, A. Iera, S. Pizzi, and F. Rinaldi, "Toward 6G non-terrestrial networks," *IEEE Network*, vol. 36, no. 1, pp. 113–120, 2022.

[9] S. Saleh et al., "Integrated 6G TN and NTN localization: challenges, opportunities, and advancements," *IEEE Communications Standards Magazine*, vol. 9, no. 2, pp. 63–71, 2025.

[10] X. Luo, H.-H. Chen, and Q. Guo, "LEO/VLEO satellite communications in 6G and beyond networks – technologies, applications, and challenges," *IEEE Network*, vol. 38, no. 5, pp. 273–285, 2024.

[11] A. Vanelli-Coralli, A. Guidotti, T. Foggi, G. Colavolpe, and G. Montorsi, "5G and beyond 5G non-terrestrial networks: Trends and research challenges," in *2020 IEEE 3rd 5G World Forum (5GWF)*, 2020, pp. 163–169.

[12] M. Huang, J. Chen, and S. Feng, "Synchronization for OFDM-based satellite communication system," *IEEE Transactions on Vehicular Technology*, vol. 70, no. 6, pp. 5693–5702, 2021.

[13] Z. Shujuan, L. Xiaofeng, and J. Min, "A frequency synchronization algorithm for ofdm in mobile satellite communication systems," in *IEEE Conference Anthology*, 2013, pp. 1–4.

[14] ITU-R, "Framework and overall objectives of the future development of IMT for 2030 and beyond," International Telecommunication Union, Technical Specification (TS) M.2160-0, Nov. 2023.

[15] Q. Wei, X. Chen, Z. Ni, C. Jiang, Z. Huang, and S. Zhang, "Integrated Doppler Positioning in a Narrowband Satellite System: Performance Bound, Parameter Estimation, and Receiver Architecture," *IEEE Internet of Things Journal*, vol. 11, no. 6, pp. 10 893–10 910, 2024.

[16] W. Stock, R. T. Schwarz, C. A. Hofmann, and A. Knopp, "Survey on opportunistic PNT with signals from LEO communication satellites," *IEEE Communications Surveys & Tutorials*, vol. 27, no. 1, pp. 77–107, 2025.

[17] C. Zhao, H. Qin, N. Wu, and D. Wang, "Analysis of Baseline Impact on Differential Doppler Positioning and Performance Improvement Method for LEO Opportunistic Navigation," *IEEE Transactions on Instrumentation and Measurement*, vol. 72, pp. 1–10, 2023.

[18] J. J. Khalife and Z. M. Kassas, "Receiver design for Doppler positioning with LEO satellites," in *ICASSP 2019 - 2019 IEEE International Conference on Acoustics, Speech and Signal Processing (ICASSP)*, 2019, pp. 5506–5510.

[19] S. Amiri and M. Mehdipour, "Accurate Doppler frequency shift estimation for any satellite orbit," in *3rd International Conference on Recent Advances in Space Technologies*, 2007, pp. 602–607.

[20] H. Rouzegar and M. Ghanbarisabagh, "Estimation of Doppler curve for LEO satellites," *Wireless Personal Communications*, vol. 108, Oct. 2019.

[21] J. A. Slater and S. Malys, "WGS 84 — past, present and future," in *Advances in Positioning and Reference Frames*, ser. International Association of Geodesy Symposia, vol. 118, Springer, Berlin, Heidelberg, 1998.

[22] A. B. De F. Diniz, T. Eriksson, and U. Gustavsson, "An algorithm for harsh Doppler shift estimation for satellite communications," in *2024 58th Asilomar Conference on Signals, Systems, and Computers*, 2024, pp. 706–710.

[23] S. A. Klioner, *Basic celestial mechanics*, lecture notes at Technische Universität Dresden, `https://arxiv.org/abs/1609.00915`, 2016.

[24] M. A. Hasan, M. H. Kabir, M. S. Islam, S. Han, and W. Shin, "A double-difference Doppler shift-based positioning framework with ephemeris error correction of LEO satellites," *IEEE Systems Journal*, vol. 18, no. 4, pp. 2157–2168, 2024.

[25] J. Saroufim and Z. M. Kassas, "LEO ephemeris error modeling enabling long baseline correction for improved PNT," in *2025 IEEE/ION Position, Location and Navigation Symposium (PLANS)*, 2025, pp. 625–630.

[26] A. Al-Hourani and B. Al Homssi, "Doppler shift distribution in satellite constellations," *IEEE Communications Letters*, vol. 28, no. 9, pp. 2131–2135, 2024.

[27] S. Hayek, J. Saroufim, and Z. M. Kassas, "Analysis and correction of LEO satellite propagation errors with application to navigation," in *ION GNSS+, The International Technical Meeting of the Satellite Division of The Institute of Navigation*, Baltimore, Maryland: Institute of Navigation, Oct. 2024, pp. 1800–1811.

[28] N. Khairallah and Z. M. Kassas, "Ephemeris tracking and error propagation analysis of LEO satellites with application to opportunistic navigation," *IEEE Transactions on Aerospace and Electronic Systems*, vol. 60, no. 2, pp. 1242–1259, 2024.

[29] D. Tse and P. Viswanath, *Fundamentals of wireless communication*. USA: Cambridge University Press, 2005.

[30] A. B. d. F. Diniz, T. Eriksson, U. Gustavsson, S. Saleh, H. Wymeersch, and S. Euler, "Doppler-based geolocalization under hardware, atmospheric and orbital impairments for single LEO satellite systems," *IEEE Transactions on Aerospace and Electronic Systems*, 2026, submitted for publication.

[31] J. Wang, C. Jiang, L. Kuang, and B. Yang, "Iterative Doppler frequency offset estimation in satellite high-mobility communications," *IEEE Journal on Selected Areas in Communications*, vol. 38, no. 12, pp. 2875–2888, 2020.

[32] Q. Wei, X. Chen, and Y. F. Zhan, "Exploring implicit pilots for precise estimation of LEO satellite downlink Doppler frequency," *IEEE Communications Letters*, vol. 24, no. 10, pp. 2270–2274, 2020.

[33] 3GPP, "Study on New Radio (NR) to support non-terrestrial networks (Release 15)," 3rd Generation Partnership Project (3GPP), Technical Specification (TS) 38.811, Sep. 2020, Version 15.4.0.

[34] S. Kay, "A fast and accurate single frequency estimator," *IEEE Transactions on Acoustics, Speech, and Signal Processing*, vol. 37, no. 12, pp. 1987–1990, 1989.

[35] A. B. de Freitas Diniz, T. Eriksson, and U. Gustavsson, "Doppler shift estimation for satellite communications using linear estimators," in *2024 IEEE 25th International Workshop on Signal Processing Advances in Wireless Communications (SPAWC)*, Lucca, Italy, Sep. 2024, pp. 686–690.

[36] S. J. Nawaz, E. Cianca, T. Rossi, and M. De Sanctis, "Round trip time (RTT) and Doppler measurements for IoRT localization by a single-satellite," *IEEE Communications Letters*, vol. 28, no. 3, pp. 528–532, 2024.

[37] N. Levanon, "Quick position determination using 1 or 2 LEO satellites," *IEEE Transactions on Aerospace and Electronic Systems*, vol. 34, no. 3, pp. 736–754, 1998.

[38] F. T. McClure, *Method of navigation*, U.S. Patent 3 172 108, Assignee: U.S. Navy, Mar. 1965.

[39] J. Kouba, "Doppler positioning: Satellite," in *Geophysics*. Boston, MA: Springer US, 1990, pp. 218–223, ISBN: 978-0-387-30752-7.

[40] Z. Tan, H. Qin, L. Cong, and C. Zhao, "New method for positioning using iridium satellite signals of opportunity," *IEEE Access*, vol. 7, pp. 83 412–83 423, 2019.

[41] 3GPP, "Release 17 Description; summary of Rel-17 work items," 3rd Generation Partnership Project (3GPP), Technical Specification (TS) 21.917, Mar. 2023, Version 17.0.1.

[42] W. Stock, R. T. Schwarz, and A. Knopp, "Error source analysis for Doppler shift based opportunistic LEO-PNT with Starlink signals," in *2025 IEEE/ION Position, Location and Navigation Symposium (PLANS)*, 2025, pp. 774–781.

[43] 3GPP, "Study on requirements and use cases for network verified UE location for Non-Terrestrial-Networks (NTN) in NR," 3rd Generation Partnership Project (3GPP), Technical Specification (TS) 38.882, Jun. 2022, Version 18.0.0.

[44] P. B. Ellis and F. Dowla, "Single satellite emitter geolocation in the presence of oscillator and ephemeris errors," in *2020 IEEE Aerospace Conference*, 2020, pp. 1–7.

[45] T. Amishima, "Switching-based FOA geolocation method with frequency offset by a single moving observation platform," *IEICE TRANSACTIONS on Communications*, vol. E108-B, no. 4, pp. 374–383, Apr. 2025, ISSN: 1745-1345.

[46] S. Mandelli, M. Magarini, and A. Spalvieri, "Modeling the filtered and sampled continuous-time signal affected by Wiener phase noise," in *2014 19th European Conference on Networks and Optical Communications - (NOC)*, 2014, pp. 173–178.

[47] A. Demir, A. Mehrotra, and J. Roychowdhury, "Phase noise in oscillators: A unifying theory and numerical methods for characterization," *IEEE Transactions on Circuits and Systems I: Fundamental Theory and Applications*, vol. 47, no. 5, pp. 655–674, 2000.

[48] B. Gävert, M. Coldrey, and T. Eriksson, "Phase noise estimation in OFDM systems," *IEEE Transactions on Communications*, vol. 73, no. 6, pp. 4349–4362, 2025.

[49] L. Bian, "Study on ionospheric delay correction in GPS signal," in *2013 IEEE 11th International Conference on Electronic Measurement & Instruments*, vol. 1, 2013, pp. 79–83.

[50] C. Shi, Y. Zhang, and Z. Li, "Revisiting Doppler positioning performance with LEO satellites," *GPS Solutions*, vol. 27, no. 126, 2023.

[51] P. Gogas, T. Papadimitriou, and E. Takli, "Comparison of simple sum and divisia monetary aggregates in GDP forecasting: a support vector machines approach," *Economics Bulletin*, vol. 33, pp. 1101–1115, 2013.